ELSEVIER

Ceramics International 31 (2005) 267–270

CERAMICS INTERNATIONAL

www.elsevier.com/locate/ceramint

AlN–TiB_2 composites fabricated by spark plasma sintering

Xiang-Yu Zhang*, Shou-Hong Tan, Dong-Liang Jiang

State Key Laboratory of High Performance Ceramics and Superfine Microstructure, Shanghai Institute of Ceramics, Chinese Academy of Sciences, 1295 Dingxi Road, Shanghai 200050, PR China

Received 8 March 2004; received in revised form 26 March 2004; accepted 4 May 2004
Available online 9 August 2004

Abstract

Dense AlN–TiB_2 composites doped with Y_2O_3 were prepared by spark plasma sintering. X-ray diffraction and transmission electron microscopy analyses show that no TiN was formed in the sintering process while BN was formed. The maximum values of hardness and toughness were up to 15.0 GPa and 5.6 MPa $m^{1/2}$, respectively. The improved toughness is considered to be mainly associated with the crack deflection due to a weak interface between AlN and TiB_2 as well as a high resistance to crack propagation in the AlN matrix region due to a large residual compressive stress from thermal expansion mismatch between AlN and TiB_2.

Keywords: A. Sintering; B. Composites; C. Toughness and toughening

1. Introduction

AlN ceramics attract growing interest for their high thermal conductivity and good electrical properties in recent years. According to the microstructure and chemical composition of the sintered ceramics, thermal conductivity of AlN ceramics varies between 80 and 260 W m^{-1} K^{-1} [1–3]. Besides high thermal conductivity, AlN ceramics exhibit good electrical insulation, low dielectric constant and low thermal expansion coefficient. It is commonly recognized that AlN ceramics are considerably potential substrate materials. In addition, AlN ceramics have various structural and refractory applications.

Titanium diboride (TiB_2) has a high melting point (2850–2900 °C), and exhibits high chemical inertness at high temperature. It also has high electrical conductivity [4]. All these characteristics make it a good candidate for special electrical applications, e.g., the cathodes used in aluminum electro-melting or the vaporizing elements for vacuum metal deposition installations [5,6]. Xu et al. [7] recently reported microwave sintering of the composites of AlN and TiB_2 developed to be used in vacuum electronic devices and particle accelerators to suppress parasitic electromagnetic oscillations and damp higher order modes.

In the present study, for the first time, composites of AlN and TiB_2 were sintered by spark plasma sintering (SPS) to evaluate the applicability of SPS techniques in compacting the AlN–TiB_2 composites. The mechanical properties were investigated and correlated to the microstructure and the composition.

2. Experimental

Commercially available AlN (Haineng Co., China), TiB_2 (Bangde Co., China), Y_2O_3 (Yuelong Co., China) were used as the starting powders. The mean particle sizes of AlN and TiB_2 were 5 and 2.5 μm, respectively. They were blended in ethanol in an attritor with SiC balls for 6 h to yield a series of AlN–TiB_2–Y_2O_3 mixtures with TiB_2 wt.% of 10, 20, 30, 40, and 50. After drying at 60 °C for 8 h, the blended powders were screened through a 100-mesh sieve. Each of the resulted powders was put into a graphite die with an inner diameter of 25 mm and then sintered in a SPS apparatus (SPS-2040, Sumitomo Coal Mining Co., Japan) under a uniaxial pressure of 30 MPa in vacuum. The heating rate

* Corresponding author. Tel.: +86 21 52414202; fax: +86 21 52413903.
E-mail address: x.y.zhang@263.net.cn (X.-Y. Zhang).

0272-8842/$30.00
doi:10.1016/j.ceramint.2004.05.013

Table 1
Compositions preparation conditions and densities of the composites

Material	Starting powders (wt.%)			Preparation conditions			Measured density (g cm^{-3})	Theoretical density (g cm^{-3})
	AlN	TiB_2	Y_2O_3	Sintering temperature (°C)	Holding time (min)	Pressure (MPa)		
T0	94	0	6	1600	4	30	3.27	3.33
T10	84	10	6	1600	4	30	3.35	3.41
T20	74	20	6	1600	4	30	3.43	3.49
T30	64	30	6	1560	4	30	3.55	3.58
T40	54	40	6	1550	4	30	3.63	3.68
T50	44	50	6	1540	4	30	3.71	3.78

was 150 °C min^{-1} for all the sintering. The processing conditions for the SPS sintered materials are summarized in Table 1.

The densities of the resulting samples were measured according to the Archimedes' method. The hardness (H_V) and indentation fracture toughness (K_{IC}) of the samples were measured at room temperature by the Vickers diamond indentation method under a load of 98 N and evaluated by the equations given by Evans and Charles [8] after being carefully polished by standard diamond polishing techniques down to 1 μm finish. The crystalline phases were characterized by X-ray diffraction (XRD, RAX-10, Rigaku, Japan) with Cu Kα radiation. Scanning electron microscopy (SEM, EPMA-8705QH2) and transmission electron microscopy (TEM, JEM-2010, JEOL, Japan) equipped with energy-dispersive spectroscopy (EDS) were employed to examine the microstructure.

3. Results and discussion

All the samples were densified to near-theoretical densities, with values of higher than 98% TD (Table 1). XRD analysis shows that AlN and TiB_2 are the major phases for all of the AlN–TiB_2 composites, and $YAlO_3$ (YAP) and $Y_3Al_5O_{12}$ (YAG) are the main secondary phases dependent on the ratio of AlN and Y_2O_3. No peaks of TiN and BN were found. This result is different from that of the microwave sintered AlN–TiB_2 composites [7]. In the latter case, TiN peaks were found in the XRD pattern of samples sintered under argon atmosphere, while both TiN and BN were found in the XRD pattern of samples sintered under nitrogen atmosphere.

Fig. 1 shows the SEM graphs of polished surfaces of the AlN–TiB_2 composites. The AlN was composed of grains about 3 μm with a yttria-based secondary phase. The grains in AlN–TiB_2 composites consisted of randomly dispersed 3 μm TiB_2 grains in the AlN matrix. Compared to the grain size of attrited powders, the AlN and TiB_2 grains had not grown much, which may be because the sintering time was too short. EDS analysis showed that dispersed gray particles are TiB_2 and the white is a yttria-based secondary phase.

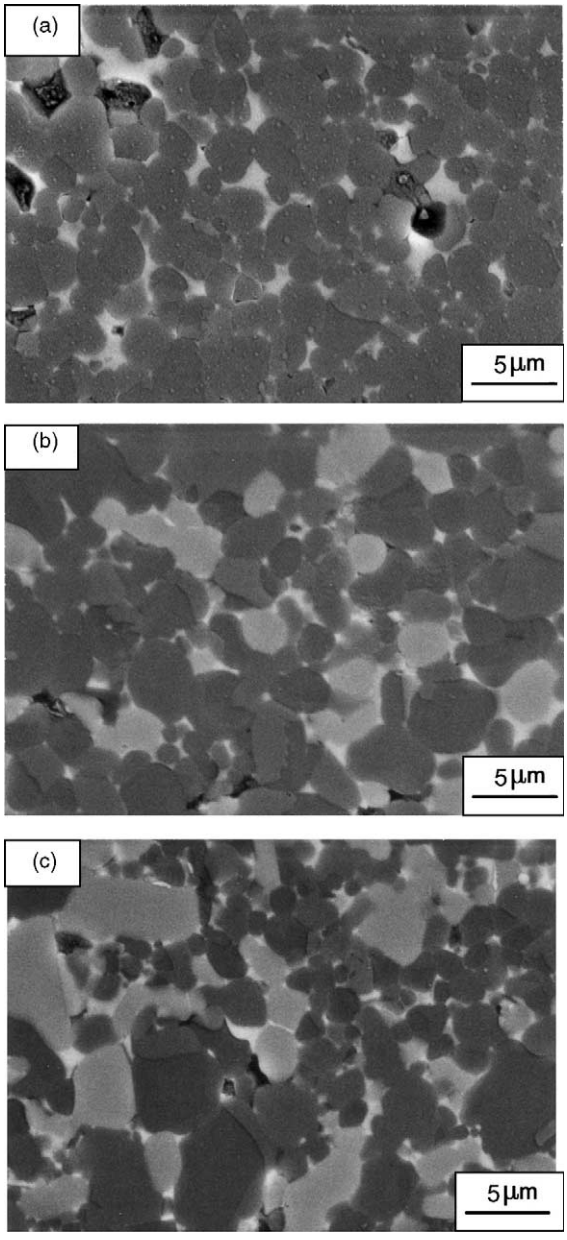

Fig. 1. SEM micrographs of polished surfaces in AlN–TiB_2 composites with various TiB_2 contents: (a) 0, (b) 20, and (c) 40 wt %. The black grains are AlN; the gray ones are TiB_2; the white is a yttria-based secondary phase.

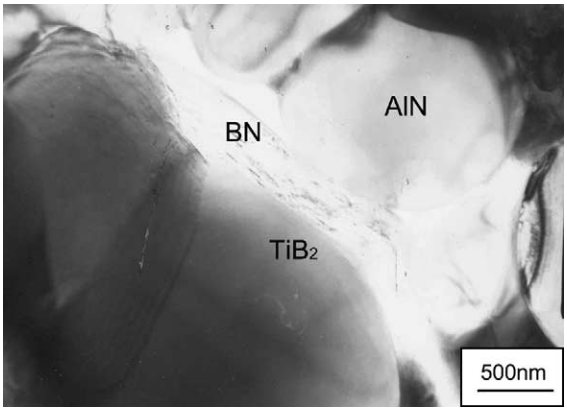

Fig. 2. TEM image of sample T40, showing the existence of BN.

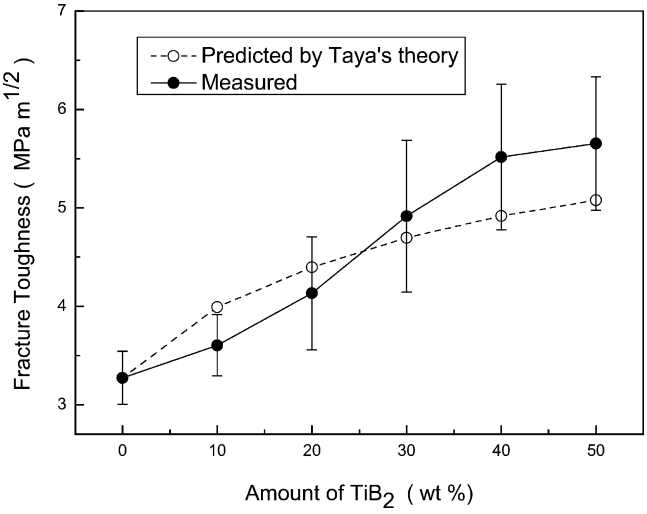

Fig. 4. Fracture toughness of AlN–TiB_2 composites vs. TiB_2 content.

Although BN was not detected by XRD, TEM investigation found the existence of BN in the sample with 40 wt.% TiB_2, as shown in Fig. 2. Similar morphology was also observed from other samples with different amounts of TiB_2. The presence of TiN was not detected by TEM, which is consistent with the XRD analysis.

Vickers hardness and fracture toughness are plotted as a function of TiB_2 wt.% in Fig. 3 and Fig. 4 (solid curve), respectively. The hardness of monolithic AlN is about 10.6 GPa. The hardness increased approximately 41% when adding 50 wt.% TiB_2. The calculated hardness according to the rule of mixtures is also included in Fig. 3. In the calculation, the hardness of AlN (10.6 GPa) is obtained from the measurement and that of TiB_2 (25 GPa) is from the literature [9]. The measured values of hardness are lower than the calculated but the trend is similar. Compared to the fracture toughness of AlN measured in the present work (about 3.2 MPa $m^{1/2}$), the fracture toughness increased approximately 73% when adding 50 wt.% TiB_2, giving the value of about 5.6 MPa $m^{1/2}$. The dash curve in Fig. 4 will be discussed later.

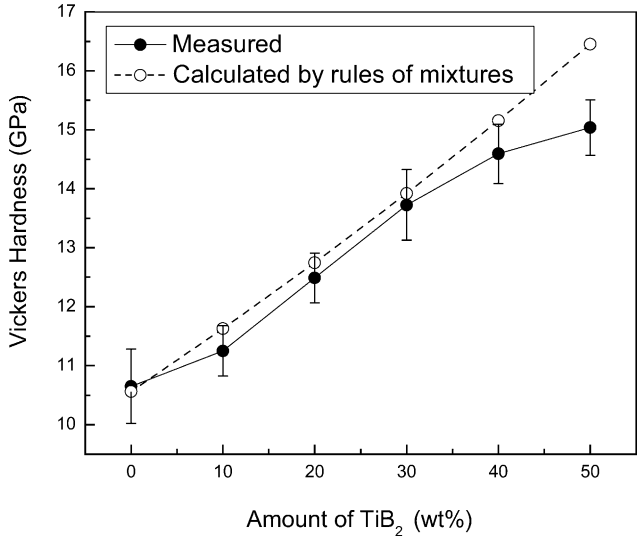

Fig. 3. Vickers hardness of AlN–TiB_2 composites vs. TiB_2 content.

Fig. 5(a–c) shows the mode of crack propagation on the polished surfaces of monolithic AlN and AlN–TiB_2 composites derived by the indentation. A comparison between the three figures reveals that monolithic AlN and AlN–TiB_2 composites both exhibit a crack deflection during crack propagation. However, the degree of crack deflection is not the same. In monolithic AlN, although the cracks propagate mainly along the AlN grains boundary as was shown in Fig. 5(a), the cracks across the AlN grains are found. As shown in Fig. 5(b) and Fig. 5(c), in AlN–TiB_2 composites, the cracks preferentially propagate along the TiB_2 grain boundary and the crack deflection of the composites is more significant than that of monolithic AlN.

Possible reasons responsible for the crack-propagation behavior may result from the thermal expansion coefficient mismatch between AlN ($4.4 \times 10^{-6}\,K^{-1}$) [10] and TiB_2 ($7.4 \times 10^{-6}\,K^{-1}$) [9]. First, as a result of the thermal expansion coefficient mismatch, a change of residual stress across the interface, from compression (in the AlN matrix) to tension (in the TiB_2 reinforcements), might cause a weak interface bonding between the TiB_2 and AlN grains. Second, a large residual compressive stress from thermal expansion mismatch in AlN matrix creates a high resistance to crack propagation in the matrix region. At the same time, as suggested by Xu et al. [7], the expansion coefficient mismatch between the matrix AlN and the TiB_2 reinforcements might cause a stress field interacting with the crack front around TiB_2 particles after cooling from the sintering temperature. The predicted values of fracture toughness based on the theory of Taya et al. [11] are illustrated in Fig. 4 (dash curve), showing that the model agrees roughly with the experiment. And finally, as observed by TEM, the weak interface due to the formation of BN between AlN and

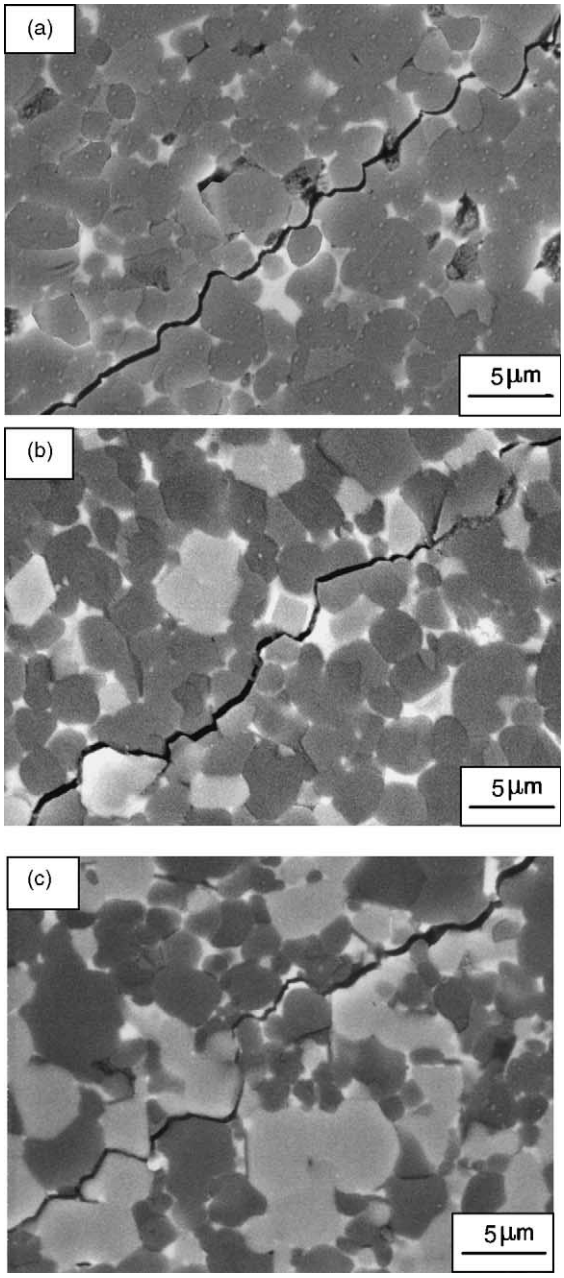

Fig. 5. SEM micrographs of cracks resulting from the Vickers indentation on polished surfaces of AlN–TiB_2 composites with various TiB_2 contents (a) 0, (b) 20, and (c) 40 wt.%.

TiB_2 grains may also contribute to the crack-propagation behavior.

4. Conclusion

Dense AlN–TiB_2 composites doped with Y_2O_3 were obtained by SPS between 1540 and 1610 °C under a uniaxial pressure of 30 MPa in vacuum. TEM analysis shows that BN was formed in the sintering process. No TiN was found for all the samples. The mechanical properties (Vickers hardness, indentation fracture toughness) of the composites were improved by the addition of TiB_2, and increased with the amount of TiB_2 addition, exhibiting the hardness of 11.2–15.0 GPa and the fracture toughness of 3.6–5.6 MPa $m^{1/2}$. The main toughening mechanism revealed by the microstructure observation was the crack deflection.

References

[1] G.A. Slack, R.A. Tanzilli, R.O. Pohl, J.W. Vandersande, The intrinsic thermal conductivity of AlN, J. Phys. Chem. Solids 48 (7) (1987) 641–647.
[2] L.M. Sheppard, Aluminium nitride: a versatile but challenging material, Am. Ceram. Soc. Bull. 69 (11) (1990) 1801–1812.
[3] A.V. Virkar, T.B. Jackson, R.A. Cutler, Thermodynamic and kinetic effects of oxygen removal on the thermal conductivity of aluminum nitride, J. Am. Ceram. Soc. 72 (11) (1989) 2031–2042.
[4] C. Mroz, Titanium diboride, Am. Ceram. Soc. Bull. 74 (6) (1995) 158–159.
[5] J.B. Todd, Energy reduction in Hall–Heroult cells with conventional and special electrodes, J. Met. 33 (9) (1981) 42–45.
[6] H.R. Baumgartner, Mechanical properties of densely sintered high purity titanium in molten aluminum environments, J. Am. Ceram. Soc. 67 (7) (1984) 490–497.
[7] G.-F. Xu, Y. Carmel, T. Olorunyolemi, I.K. Lloyd, O.C. Wilson Jr., Microwave sintering and properties of AlN/TiB_2 composites, J. Mater. Res. 18 (1) (2003) 66–76.
[8] A.G. Evans, E.A. Charles, Fracture toughness determined by indentation, J. Am. Ceram. Soc. 59 (7/8) (1976) 371–372.
[9] R.G. Munro, Material properties of titanium diboride, J. Res. Natl. Inst. Stand. Technol. 105 (5) (2000) 709–720.
[10] N. Kuramoto, H. Taniguchi, I. Aso, Development of translucent aluminum nitride ceramics, J. Am. Ceram. Soc. 68 (4) (1989) 883–887.
[11] M. Taya, S. Hayashi, A.S. Kobayashi, H.S. Yoon, Toughening of particulate-reinforced ceramic-matrix composite by thermal residual stress, J. Am. Ceram. Soc. 73 (5) (1990) 1382–1391.